**Hydrocarbon seepage during the Messinian salinity crisis in the Tertiary Piedmont Basin (NW Italy)**

UNIVERSITÀ DEGLI STUDI DI TORINO

# Hydrocarbon seepage during the Messinian salinity crisis in the Tertiary Piedmont Basin (NW, Italy)

Marcello Natalicchio[a]*, Francesco Dela Pierre[a,b], Pierangelo Clari[a], Daniel Birgel[c], Simona Cavagna[a], Luca Martire[a], Jörn Peckmann[c]

[a]*University of Torino, Department of Earth Sciences, 10125 Torino, Italy*

[b]*CNR-IGG, 10125 Torino, Italy*

[c]*University of Vienna, Department of Geodynamics and Sedimentology, Center for Earth Sciences, 1090 Vienna, Austria*

*Corresponding author:

marcello.natalicchio@unito.it

phone:

+390116705198

Fax:

+390116705339

ABSTRACT

Seep carbonate deposits of Messinian age have been recently found in the Tertiary Piedmont Basin (NW Italy). These carbonates are preserved as blocks within a chaotic unit emplaced during the Messinian salinity crisis (MSC). They show negative $\delta^{13}C$ values (from −27 to −15‰ VPDB) that indicate the involvement of hydrocarbon-rich fluids in their genesis. Three types of carbonates are recognised: (i) vuggy carbonates; (ii) *Lucina* carbonates; (iii) tubeworm carbonates. Vuggy carbonates are characterised by carbonate pseudomorphs after gypsum and probably formed during the first stage of the MSC. They are the product of a complex diagenesis, influenced by both hypersalinity and seepage of hydrocarbon rich fluids. These rocks lack chemosymbiotic assemblages, reflecting their formation under extreme environmental conditions, inhospitable for most metazoans. In contrast, *Lucina* and tubeworm carbonates are characterised by containing chemosymbiotic macrofauna, represented respectively by *Lucina* bivalves and vestimentiferan tubeworms. The latter have not commonly been documented in ancient seep carbonates and have never been reported from the Messinian sediments of the Piedmont Basin. Both *Lucina* and tubeworm carbonates are interpreted as the product of hydrocarbon seepage during the second MSC stage. These two types of carbonates formed under less severe conditions than the vuggy carbonates, allowing the survival of seep-dwelling metazoans. During the second MSC stage, the seafloor was probably characterised by an irregular topography and a thin bottom layer of dense anoxic brines, produced by the dissolution of gypsum. It is suggested that vestimentiferan worms were able to thrive on morphologic highs with the posterior part of tubes just below the oxic-anoxic interface, but the anterior part projecting into oxic water. The infaunal *Lucina* bivalves were only able to live were seeps occurred in parts of the seafloor placed above the oxic-anoxic boundary. The studied carbonate deposits show features reflecting the uncommon interaction of hydrocarbon-rich seep fluids and sulphate-enriched waters – the latter resulting from both evaporation and dissolution of gypsum – and allow to reconstruct the evolution of a seepage system during the MSC.

*Keywords:*
Seep carbonates
Hypersaline conditions
Vestimentiferan tubeworms
Messinian salinity crisis

## 1. Introduction

Cold seeps are sites of localized expulsion of hydrocarbons at the seafloor, predominantly composed of methane or higher hydrocarbons, and containing locally generated hydrogen sulphide. Seep deposits are widely documented in both modern (e.g. Paull et al., 1992; Aloisi et al., 2000; Levin, 2005; Mazzini et al., 2008) and ancient marine depositional settings (e.g. Peckmann et al., 1999; Clari et al., 2004, 2009; Peckmann and Thiel, 2004; Campbell 2006). Marine seeps and their deposits are characterised by several diagnostic features including: (i) authigenic minerals, mainly consisting of carbonates like calcite, aragonite, and dolomite (e.g. Ritger et al., 1987; Paull et al., 1992; Aloisi et al., 2002), (ii) negative $\delta^{13}C$ values (as low as −75‰ VPDB; Campbell, 2006) of early diagenetic authigenic carbonate phases; (iii) chemosymbiotic macro-fauna (dominated by bivalves and vestimentiferan tubeworms), and (iv) a characteristic prokaryotic community represented by methanotrophic archaea, sulphate-reducing bacteria, as well as mat-forming sulphide-oxidising bacteria, and thiotrophic or methanotrophic endosymbionts in chemosymbiotic seep metazoans (e.g., Boetius et al., 2000; Orphan et al., 2002; Duperron et al., 2005). The distribution and the biological activity of the various chemosymbiotic organisms is controlled by parameters such as (i) water depth, (ii) fluid composition, (iii) fluid emission rate, (iv) occurrence of gas hydrates, and (v) sulphide contents (Levin, 2005; Olu-Le Roy et al., 2007; Cordes et al., 2010).

In Cenozoic successions of the Mediterranean, cold seep carbonates are widely distributed and have been described in detail (e.g. Conti and Fontana, 2005; Clari et al., 2009). These carbonates have been reported in strata as old as Eocene (Venturini et al., 1998) in various basin types including foredeep, episutural, and foreland basins (e.g. Ricci Lucchi and Vai, 1994). In most cases, such carbonates consist of extensively cemented blocks and lenses, which are mostly hosted in deep-water claystones and siltstones. The largest seep deposits and the highest diversity of chemosymbiotic macrofauna are observed in Upper Serravallian-Tortonian sediments, reflecting intense hydrocarbon seeping at that time (e.g. Taviani, 2001, 2011). Such Miocene carbonates are commonly characterised by chemosymbiotic macrofauna dominated by *Lucina* clams. In contrast, only very few seep carbonates have been reported from the Messinian salinity crisis (MSC) stratigraphic record (e.g. Clari et al., 2004, 2009).

The present paper describes cold seep deposits discovered within the Messinian sediments of the eastern margin of the Tertiary Piedmont Basin (Fig. 1A). This discovery provides the opportunity to trace the evolution of methane seepage into the MSC. The studied deposits contain macro-fossil assemblages and show sedimentological, petrographic, and geochemical features, that reveal an uncommon interaction of hydrocarbon-rich seep fluids and sulphate-enriched waters resulting from both seawater evaporation and dissolution of gypsum deposits.

## 2. The Messinian salinity crisis

The MSC is a major palaeo-oceanographic event that occurred about 6 my ago. In its course the Mediterranean was transformed into one of the largest salt basins in Earth history (e.g. CIESM, 2008). After the discovery of the deep-seated Mediterranean evaporites (Hsü et al., 1973), mostly buried below the abyssal plains of the present day Mediterranean sea, a multitude of studies has been carried out on the Messinian Mediterranean succession, resulting in different and sometimes contrasting interpretations of the MSC (e.g. Rouchy and Caruso, 2006; CIESM, 2008). Recently, a

new scenario for the MSC was proposed (CIESM, 2008; Roveri et al., 2008). This scenario envisages that the MSC developed through three main evolutionary stages (Fig. 2). During the first stage (from 5.96 to 5.60 Ma), sulphate evaporites (Primary Lower Gypsum unit, PLG; Roveri et al., 2008) formed in shallow-silled peripheral basins (e.g. Sorbas Basin, parts of the Tertiary Piedmont Basin, Vena del Gesso Basin of Northern Apennines), whereas in deep basinal areas organic-rich shales, interbedded with carbonate-rich layers, were deposited (e.g. parts of the Tertiary Piedmont Basin, Northern Apennine foredeep, Caltanissetta Basin of Sicily; Manzi et al., 2007, 2011; Dela Pierre et al., 2011, 2012). In the second stage (from 5.60 to 5.53 Ma), the PLG unit underwent subaerial exposure and erosion caused by a prominent sea level drop (MSC acme); the products of erosion were transferred downslope and deposited in deep basins by various types of gravity flows. These sediments, referred to as Resedimented Lower Gypsum (RLG unit, Manzi et al., 2005, 2007; Roveri et al., 2008), locally host thick halite bodies (e.g. Caltanisetta Basin). During the third stage (from 5.53 to 5.33 Ma), a cyclic alternation of gypsum and shales with brackish-water fossil assemblages (Upper Evaporites) was deposited in the SE part of the Mediterranean basin (Sicily, Ionian Islands, Crete, Cyprus, and Nile Delta area), whereas shallow to deep water clastic sediments are found in the Apennines and in the Sorbas Basin. In the upper part of these units, fresh and brackish water sediments with Paratethyan fossil assemblages are present, recording the so called Lago-Mare event (e.g. Orszag Sperber, 2006). The overlying Zanclean (Pliocene) clays record the re-establishment of fully marine conditions at the end of the MSC.

## 3. Geological setting and stratigraphy

The study area is located at the eastern margin of the Tertiary Piedmont Basin (TPB), a large wedge top basin filled with up to 5000 m of Eocene to Messinian sediments (e.g. Mosca et al., 2009; Fig. 1A). This area is bordered to the north by the Villalvernia-Varzi line, a regional structural feature that was active during Oligocene and Miocene times (Fig. 1B). The upper

Miocene succession is composed of outer shelf (Tortonian) to slope deposits (lower Messinian) referred to as the Sant'Agata Fossili Marls (Ghibaudo et al., 1985). The lower Messinian part of this succession encloses a wide array of diagenetic carbonates, including methane-derived carbonates. These carbonates result from complex processes, including bacterial sulphate-reduction, archaeal methanogenesis, as well as microbial anaerobic oxidation of methane fuelled by vigorous methane flux most likely triggered by gas hydrate destabilisation (Dela Pierre et al., 2010; Natalicchio et al., 2012). The carbonates formed both at the seafloor, giving rise to *Lucina*-bearing mud breccias, as well as in the shallow subsurface, resulting in various types of concretions that lack remains of chemosymbiotic metazoan. The topmost part of the Sant'Agata Fossili Marls consists of euxinic shales barren of fossils interpreted as the deeper water equivalent of the PLG unit deposited in shallower and marginal sectors of the basin during the first MSC stage. The PLG unit is not preserved in the study area, but was reported from the southern and northern margin of the basin, where it consists of different types of gypsum lithofacies (Dela Pierre et al., 2011). Above an erosional surface, the Sant'Agata Fossili Marls are overlain by the Valle Versa Chaotic Complex (VVCC). The latter unit, which is up to 300 metre thick, is equivalent to the RLG unit recognised in many Mediterranean sub-basins, deposited during the second stage of the MSC (e.g. Gorini et al, 2005; Lofi et al., 2005; Bertoni and Cartwright, 2007). Its origin has been attributed to large scale slope failures, probably triggered by thrusting during the intra-Messinian tectonic phase (Dela Pierre et al., 2007; Fig. 2). In the study area the VVCC is made up of three superposed intervals suggesting that the emplacement of the VVCC was polyphasic and resulted from different gravitative events. From bottom to top the VVCC sequence consists of: (i) gypsrudites and massive pebbly gypsarenite about 3 metre thick; (ii) large blocks up to tens of m in diameter of both massive and banded selenite separated by a scarce fine-grained matrix; (iii) blocks of selenite gypsum and methane-derived carbonate rocks floating in a volumetrically dominant matrix, making up an interval of as much as 80 m in thickness (Figs. 2, 3). The methane-derived carbonate blocks are the object of this study. The VVCC is overlain by the Cassano Spinola Conglomerates (upper

156 Messinian), consisting of deltaic to lagoonal brackish water sediments that are equivalent to the
157 "Lago Mare" interval deposited during the third stage of the MSC.
158
159 **4. Methods**
160
161 The lithology and geometry of the studied methane-derived carbonates was described in the
162 field by selecting 10 representative samples for further petrographic and geochemical studies. After
163 cutting and polishing carbonate samples, 15 standard petrographic thin sections were prepared.
164 Petrographic and cathodoluminescence observations were carried out by plane-polarized and cross-
165 polarized light microscopy using a CITL 8200 mk3 equipment, operating at about 17 kV and 400
166 μA. Thin sections were further analysed for their UV-fluorescence, using ultraviolet light
167 (illumination source 450-490 nm) performed on a Nikon microscope with a UV-2A filter block.
168 Scanning electron microscopy (SEM) was carried out on slightly etched polished rock surfaces,
169 obtained from the same samples used for thin section preparation, using a SEM Cambridge
170 Instruments Stereoscan 360 equipped with an energy-dispersive (EDS) microprobe Link System
171 Oxford Instruments. Microdrilled samples were measured for their carbon and oxygen stable
172 isotope composition (Tab. 1), following the method of McCrea (1950), using Finnigan MAT 251
173 and 252 mass spectrometers. The isotopic ratios are expressed as $\delta^{13}C$ and $\delta^{18}O$ values relative to
174 the VPDB standard (precision < ±0.05‰). The isotope analyses were performed in the *ISO4*
175 Laboratory (Turin, Italy) and in the *MARUM* Stable Isotope Laboratory (Bremen, Germany).
176
177 **5. Results**
178
179 Three types of carbonates were found in the third unit of the VVCC. They have been
180 distinguished on the basis of the occurrence of inferred chemosymbiotic macroinvertebrate fossils:
181 (i) vuggy carbonates lacking macroinverterbrate remains, (ii) *Lucina* carbonates, and (iii) tubeworm

carbonates. In the following sections the petrographic and the stable isotope patterns of these three categories of carbonates are described.

### *5.1. Petrography*

#### *5.1.1. Vuggy carbonates*

Vuggy carbonates consist of irregularly shaped blocks, ranging from few decimetres to several metres in size (Fig. 4A); their relationship with the encasing sediments is unclear due to poor outcrop conditions. Locally, the vuggy carbonates are interbedded with laminated siltstone (Fig. 4A) containing remains of euryhaline fishes (*Aphanius crassicaudus*, G. Carnevale, pers comm.; Fig. 4B). The vuggy carbonates are composed of silty-mudstones (Fig. 4C) cemented by intergranular dolomite crystals with a rounded, anhedral habit, whose sizes range from 5 to 20 μm (Fig. 5D). Microprobe analyses revealed that these crystals are non-stoichiometric calcium-rich dolomite. Some crystals exhibit a central hollow (Fig. 5D). Filaments, up to 1 millimetre long and 100 μm in diameter, are common (Figs. 5A,B). They are composed of micrite and contain abundant terrigenous grains including clay particles and mica flakes.

A prominent feature of vuggy carbonates is the presence of several cavities ranging from 0.2 to 3 cm in size. They show elongated and prismatic shapes (Figs. 5A,C), indicating their origin from the dissolution of gypsum crystals. The cavities are either empty or filled with sediments, polyphasic calcite cements, or some residual gypsum (Fig. 5A). The carbonate cements filling the cavities consist of polyphasic calcite cements with a colour range from white to brown under transmitted light, and bright orange to dull brown under cathodoluminescence. The entire rock is crosscut by a fracture system filled with polyphasic carbonate cements (Fig. 5C).

#### *5.1.2. Lucina carbonates*

In the study area, the *Lucina* carbonates consist of blocks up to 10 m in diameter, composed of cemented mud breccias. These carbonates can be referred to as "Calcari a *Lucina*" (*sensu* Clari et al., 1988), which have been recognised in other sectors of the TPB and in the northern Apennines (e.g. Taviani, 1994; Conti and Fontana, 2005; Clari et al., 2009). They contain fossils of putative chemosymbiotic bivalves, represented by internal moulds of articulated lucinids, whose size ranges from 3 to 15 cm (Fig. 6). The rocks are made up of centimetre-sized rounded and angular clasts, consisting of wackestones with a characteristic light brown colour. The matrix around the clasts is composed of fine-grained sediments. The intergranular cement of both clasts and matrix is represented by microcrystalline calcite. Pyrite is frequently found as framboids within the matrix, but some other pyrite was obviously oxidised. Firm ground burrows are commonly observed in this lithology. In addition to the chemosymbiotic fauna, the fossil content consists of planktic and minor benthic foraminifers. These rocks are cross-cut by a network of well-defined millimetre to centimetre thick fractures, filled with micritic sediments and carbonate cement. Cement is mainly represented by botryoidal aragonite growing directly on the fracture walls and by sparry calcite.

### *5.1.3. Tubeworm carbonates*

A single block of tubeworm carbonate (5 metre wide and 3 metre high) was found within the VVCC deposits close to large gypsum blocks (Fig. 7A). It consists of calcite-cemented mud breccias composed of mm- to dm-sized angular clasts floating in a micrite matrix (Fig. 7B). Some clasts contain abundant foraminifers and pyritized peloids, indicating their derivation from the underlying pre-Messinian succession. An intricate network of fractures cross-cut the rock matrix. The fractures are filled with pink to white-coloured carbonate cements that are mainly composed of fibrous aragonite and blocky calcite.

The most remarkable feature of this type of carbonate is a large cluster of tubular structures (Figs. 7C-D). The tubes are curved along their length, are 4 to 7 mm in cross section (Figs. 8A), and reveal a maximum exposed length of 4 cm. Tube wall thickness varies from 30 to 80 μm (Figs. 8A-

B). Walls consist of concentric dark brown to red micritic laminae 5 to 10 μm in thickness, separated from each other by cryptocrystalline calcite and small fibrous aragonite crystals (Figs. 8C-D), resulting in a delamination pattern of individual layers of the tube wall. The concentric lamination of the tube walls is also recognised by electron microscopy, revealing thin parallel but separated laminae, in places bridged by carbonate pillars (Figs. 8E-F). Tubes are partially filled with clotted micrite, characterised by closely-packed, curved elongated rods up to 1.2 millimetre long and 120 μm in diameter (Figs. 9A-C). These rods are composed of dark micrite that shows a bright fluorescence (Fig. 9D). The outer and inner surfaces of the tube walls, as well as the outer margins of aggregates of tube-filling clotted micrite are commonly coated by concentric micro-spherulites (Figs. 9B-C) that occur as isolated spherulites or form densely-packed chains and aggregates. The spherulites exhibit a hollow nucleus of spherical or dumbbell shape (Fig. 9B). The concentric zonation of spherulites is made up of turbid inner rims of dolomite and outer rims of calcite. The average diameter of the spheroids is 80 μm, the diameter of the empty nuclei ranges from 10 to 30 μm. The central portion of the tubes is partially filled with fans of acicular crystals of aragonite and late equant calcite spar (Figs. 8A-B).

### *5.2. Carbon and oxygen stable isotopes*

Thirty samples of the VVCC carbonates have been analysed for their carbon and oxygen stable isotope compositions. Both the intergranular and the cavity and fracture-filling cements have been analysed (Tab. 1; Fig. 10). The carbonate phases are marked by negative $\delta^{13}C$ values ranging from −26.7 to −14.3‰ and by $\delta^{18}O$ values ranging from −7.2 to +8.1‰. The strongest $^{13}C$-depletion was found for the vuggy carbonates, both for the spheroidal dolomite representing intergranular cement of the matrix (−26.7‰) and the fracture-filling carbonate cements (−25.0‰). Vuggy carbonates are also characterised by wide fluctuations of $\delta^{18}O$ values spanning from −6 to +1.5‰ in the microcrystalline matrix and from −7.2 to +4.4‰ in the cavity-filling cements. The

intergranular cements of both *Lucina* and tubeworm carbonates yielded negative $\delta^{13}C$ values too (as low as −26‰; Fig. 10). Positive $\delta^{18}O$ values characterise these cements with a highest value of +8.1‰ found for the tubeworm carbonates. Low $\delta^{18}O$ values were only recognised in the late diagenetic calcite cements filling cavities of the tubeworm carbonates (−5.6‰) or fractures of the *Lucina* carbonates (−4.0‰).

## 6. Discussion

The authigenic carbonates discovered in the Messinian chaotic deposits of the studied sector of the TPB show textural, petrographical, and geochemical features that, when considered together, indicate that they are cold seep deposits: (i) authigenic carbonate phases are common, both in the sediment pore space (mainly calcite and dolomite) and in open fractures (mainly aragonite and calcite), (ii) specific micro-fabrics such as clotted micrite (cf. Riding, 2000; Peckmann et al., 2002) as well as spheroidal and dumbbell-shaped crystal aggregates (cf. Cavagna et al., 1999; Peckmann et al., 1999; Peckmann and Thiel, 2004) with intense autofluorescence were recognised, suggesting a microbial origin of the carbonates, (iii) authigenic carbonates show negative $\delta^{13}C$ values (ranging from −27 to −14‰). Compared to other methane-derived carbonates, which can reveal $\delta^{13}C$ values as low as −75‰ (Campbell, 2006), the moderate $^{13}C$ depletion observed in the VVCC rocks can be explained with a mixture of methane-derived carbon with other sources, such as, marine dissolved inorganic carbon, or carbon deriving from the remineralisation of organic matter or heavier hydrocarbons (Roberts and Aharon, 1994). An additional cause for the moderate $^{13}C$ depletion could be a thermogenic methane source (see below). Lipid biomarkers of prokaryotes involved in the anaerobic oxidation of methane extracted from the VVCC carbonates confirm that methane oxidation contributed to carbonate formation (unpubl. data). Moreover, fracturing and brecciation testify overcritical pore water pressure during carbonate formation, possibly generated from the rising of gas-charged fluids or the destabilisation of gas hydrates (cf. Mazzini et al., 2003;

Peckmann et al., 2011; Natalicchio et al., 2012). Compared to other modern and ancient seep carbonates, but especially to those hosted in the lower Messinian slope sediments of the study area (Dela Pierre et al., 2010; Natalicchio et al., 2012), the carbonates discussed below show some very distinctive features.

### *6.1. The vuggy carbonates: evidence of hydrocarbon seepage under hypersaline conditions*

The vuggy carbonates reflect a complex evolution related to hypersalinity and seepage of hydrocarbon-rich fluids. Hypersaline depositional conditions are indicated by abundant carbonate pseudomorphs after gypsum preserved in the carbonate rocks. Most likely, gypsum grew within porous muds impregnated by oversaturated brines (Fig. 11A). The preservation of pseudomorphs suggests that the host sediments underwent an early phase of dolomite cementation close to the seafloor prior to dissolution of gypsum crystals. Primary dolomite precipitation, which is known to occur at seeps (e.g. Cavagna et al., 1999; Peckmann et al., 1999; Roberts et al., 2010) is indicated by the petrographic relationships with the surrounding sediments. The filamentous structures randomly dispersed in the sediments (Fig. 5D) may represent faecal pellets of brine shrimp of the genus *Artemia*. These faecal pellets have been reported from modern hypersaline environments (Djamali et al., 2010), but as well in Messinian sediments (e.g. Schreiber et al., 1976; Guido et al., 2007). A faecal origin of these filaments is further supported by the incorporated terrigenous grains like clay particles and mica flakes. Finally, high salinities during deposition agree with the presence of fossils of *Aphanius crassicaudus*, an euryhaline fish commonly found in the PLG unit of the first MSC stage elsewhere in the Piedmont Basin (Dela Pierre et al., 2011). Based on these observations, it seems likely that the vuggy carbonates formed during the first stage of the MSC and were redeposited during its second stage (see Fig. 2).

The intergranular dolomite cement reveals a high autofluorescence as well as spherical and dumbbell-shaped crystal habits (Figs. 5E-F). All these features suggest a microbial origin of the

311 dolomite. Similar features have been described from present day hypersaline coastal lagoons, where
312 dolomites were interpreted to be the product of the activity of sulphate-reducing bacteria (e.g.
313 Vasconcelos et al., 1995; Warthmann et al., 2000). Microbial dolomites with similar crystal habits
314 have also been reported from ancient seep deposits (e.g. Cavagna et al., 1999; Peckmann et al.,
315 1999), where dolomite precipitation was driven by the anaerobic oxidation of methane (AOM). The
316 negative $\delta^{13}C$ values (as low as −27‰) of the studied dolomites suggest a contribution of AOM to
317 dolomite precipitation (Fig. 11B). AOM consortia were probably sustained by diffusive flux of
318 methane-rich fluids and favoured by the presence of sulphate-saturated Messinian brines. The
319 absence of chemosymbiotic macro-faunal remains agrees with extreme environmental conditions,
320 inhospitable for most metazoans, but favourable for halotolerant methanotrophs (cf. Ziegenbalg et
321 al., 2012).
322 The petrographical complexity of the vuggy carbonates is caused by the successive
323 occurrence of several diagenetic events (Figs. 11C-D), including (i) the opening of a fracture system
324 crosscutting the cemented gypsum-bearing sediments, (ii) the dissolution of gypsum crystals
325 generating new porosity, and (iii) the infill of parts of the newly generated porosity with calcite
326 cements. The low carbon isotope values of the later-stage cavity-filling calcite cements confirm a
327 carbon source from hydrocarbon-rich fluids. The $\delta^{18}O$ values are difficult to interpret and could
328 reflect an intermittent influence of meteoric waters under fluctuating salinity conditions or an effect
329 of microbial sulphate consumption (AOM or organoclastic sulphate reduction) as a possible cause
330 of $^{16}O$-enrichment in the microenvironments of carbonate precipitation (cf. Sass et al., 1991;
331 Turchyn et al., 2010).
332
333 *6.2. The Lucina carbonates: evidence of hydrocarbon seepage in the shallow subsurface*
334
335 The studied *Lucina* carbonates, like many other examples in the Neogene of the
336 Mediterranean (e.g. Taviani, 1994; Clari et al., 2004, 2009; Conti et al., 2008), formed at

hydrocarbon seeps based on the co-occurrence of densely packed chemosymbiotic bivalves and negative $\delta^{13}C$ values of the authigenic carbonate minerals (av. −20‰). This type of carbonate formed in the shallow subsurface, near to the sediment-water interface, below an oxygenated seafloor. Not only are *Lucina* bivalves oxygen-dependant (Taylor and Glover, 2009), but many specimens reveal boreholes in the shells, reflecting drilling predation of oxygen-dependent predators (cf. Kelly and Hansen, 2003; Amano and Jenkins, 2007; Clari et al., 2009).

### *6.3. Tubeworm carbonates: the preservation of a colony of vestimentiferan worms*

Textural and compositional characteristics of the tubeworm carbonates (e.g. brecciation and clasts sourced from the underlying pre-Messinian successions) suggest that these features resulted from hydrocarbon-seepage associated with the extrusion of unconsolidated fine-grained sediments onto the seafloor, as previously suggested for similar deposits from the pre-Messinian succession of this sector (Dela Pierre et al., 2010) and elsewhere in the Piedmont Basin (Clari et al., 2004; 2009). In contrast to the previously studied carbonates, this type of rock contains tubular structures. The tubes are interpreted as remains of vestimentiferan tubeworms on the basis of their similarity with living vestimentiferan worm tubes (see below). At modern seeps, the chemosymbiotic vestimentiferan worms commonly form dense bush-like colonies clustering around sites of vigorous methane flux. A great abundance of vestimentiferans usually points to very high sulphide concentrations (Cordes et al., 2003; Arvidson et al., 2004; Sahling et al., 2008). Living vestimentiferans are characterised by anterior tubes (often up to 1 m in length) with a great variety of shapes, including straight, curved to very coiled habits, projecting from the seafloor into the water column. The more permeable and thinner posterior part of the tubes grows into the underlying sediments, allowing the uptake of hydrogen sulphide from interstitial sources and pumping of sulphate back into the surrounding sediments. The enrichment of sulphate in the sediments is thought to accelerate AOM, promoting the precipitation of significant amount of carbonates (Julian

et al., 1999; Freytag et al., 2001; Cordes et al., 2003; Dattagupta et al., 2006, 2008; Haas et al., 2009).

Fossilized worm tubes interpreted to represent vestimentiferan tubeworms have been documented in some ancient seep carbonates (e.g. Goedert et al., 2000; Peckmann et al., 2005; Himmler et al., 2008; Hammer et al., 2011). In the Piedmont Basin, tubes of putative vestimentiferans were reported from the Monferrato area close to the study area (Peckmann et al., 1999). The tubes studied here reveal structural features that support their interpretation as remains of vestimentiferan tubeworms. The size and the curvature of the tubes are very similar to the anterior part of the tubes of modern vestimentiferans (e.g. the genus *Lamellibrachia*; Haas et al., 2009). Furthermore, the concentric lamination of tubes and the delamination of individual layers corresponds to the taphonomy of the tubes of modern (Haas et al., 2009) and ancient vestimentiferans (Peckmann et al., 2005; Himmler et al., 2008). Vestimentiferan worms are not the only seep-dwelling tubeworms with a layered tube wall (Kiel and Dando, 2009), but the only seep-dwelling worms for which taphonomical delamination has been reported to date at seeps.

Striking additional features of the tubeworm carbonates are elongated rods as well as spheroidal and dumbbell-shaped dolomitic crystal aggregates within the tubes. The origin of the elongated rods is unknown, but on the basis of their dimensions and their curved shape, they resemble the remains of sulphide-oxidizing bacteria reported from a Miocene seep deposit (Peckmann et al., 2004) and Messinian evaporitic carbonates (Olivieri et al., 2010). The studied textures are not preserved well enough to allow such an assignment, but the absence of incorporated terrigenous grains allows to exclude a faecal origin. For the dolomite spheroids a microbial origin is proposed on the basis of crystal habit and their intense fluorescence. Considering all these observations, it is suggested that the studied tubeworm carbonate formed at a site of vigorous gas emission at the seafloor, where high concentrations of hydrogen sulphide allowed the growth of dense colonies of vestimentiferan tubeworms and probably favoured large sulphur bacteria as well.

### *6.4. Evolution of a seepage system during the Messinian salinity crisis*

The eastern part of the Piedmont Basin reveals abundant methane-derived carbonates, documenting prolonged seepage of hydrocarbon-bearing fluids prior to and during the Messinian salinity crisis. The carbonates are hosted both in the pre-MSC slope deposits (Dela Pierre et al., 2010; Natalicchio et al., 2012 and reference therein) and in chaotic resedimented sediments deposited during the second MSC stage. Both the pre-MSC and MSC carbonate deposits show variable characteristics reflecting different depositional conditions of the host sediments and different diagenetic pathways. Previous studies (Dela Pierre et al., 2010; Natalicchio et al., 2012) documented that pre-MSC carbonates formed just below the seafloor, giving rise to cemented mud breccias with oligotypic assemblages of chemosymbiotic bivalves (*Lucina* sp.), as well as somewhat deeper in the shallow subsurface, resulting in a wide array of authigenic carbonates that record the upward migration of fluids. Some of the methane was apparently sourced by gas hydrate destabilisation in the sedimentary column (Dela Pierre et al., 2010). Stable carbon isotope data ($\delta^{13}C$ values ranging from −60 to −25‰) indicated that methane was mainly of a biogenic origin, even if a minor source of thermogenic methane was not excluded (Dela Pierre et al., 2010; Natalicchio et al., 2012). Moreover, the lipid biomarker inventory of the deeper-seated pre-MSC carbonates suggested that carbonate precipitation took place in multiple stages and was induced by various microbially-driven processes, including bacterial sulphate reduction, methanogenesis, and AOM (cf. Natalicchio et al., 2012). In contrast, all types of authigenic carbonates found in the VVCC show lesser $^{13}C$ depletion, suggesting the involvement of thermogenic methane sourced from deeper Mesozoic strata or more admixture of carbon from other sources than methane oxidation. Thermogenic methane possibly migrated upward along tectonic discontinuities like the close Villalvernia-Varzi line.

The spectrum of authigenic carbonates of the VVCC allows to shed light on the evolution of the seepage system during the MSC. Vuggy carbonates are the result of complex and polyphasic

415 early diagenetic events driven by AOM that occurred within sediments deposited under hypersaline
416 conditions. Their $^{13}C$ depletion agrees with AOM functioning under hypersaline conditions too (cf.
417 Ziegenbalg et al., 2012). The vuggy carbonates formed in the subseafloor, but, unlike the other
418 studied seep carbonates, they are barren of fossils of chemosymbiotic macroinvertebrates. This
419 absence was probably caused by hypersaline conditions, which hampered the life of most
420 eukaryotes, allowing only halotolerant prokaryotes and few specialized metazoans (putative
421 *Artemia* sp.) to survive. In contrast, *Lucina* and tubeworm carbonates (Fig. 2) do not show features
422 that allow their unequivocal attribution to the MSC stratigraphic record. However, the otherwise
423 absence of pre-MSC blocks within the VVCC succession makes it unlikely that these types of
424 carbonates were reworked from older deposits. Moreover, their C and O isotope signatures differ
425 significantly from those of the underlying pre-MSC seep carbonates (Fig. 10). The putative MSC
426 carbonates show a distinct $^{18}O$-enrichment (values as high as +8‰), already recognised for other
427 MSC carbonates of the VVCC from other parts of the Piedmont Basin (Clari et al., 2009). Similar
428 values have also been reported for sulphur-bearing, hydrocarbon-derived carbonates from Sicily
429 that formed during the MSC (Ziegenbalg et al., 2010).

430 An envisaged scenario of the evolution of the seepage system in the study area during the
431 MSC is shown in Fig. 12. Vuggy carbonates are considered as the lateral equivalent of the primary
432 evaporites (PLG unit) deposited during the first MSC stage in the shallower, marginal parts of the
433 Piedmont Basin (Fig. 12A; cf. Dela Pierre et al., 2011). The primary evaporites along with the
434 vuggy carbonates were subsequently eroded and partly incorporated as scattered blocks in the
435 VVCC during the second MSC stage (Fig. 12B). The *Lucina* and tubeworm carbonates, on the other
436 hand, are considered to be syndepositional products of seepage, formed during the second MSC
437 stage within the VVCC. The occurrence of seep-dwelling, putative chemosymbiotic metazoans in
438 some of the carbonate deposits indicates that long-lasting fluid expulsion affected a rugged seafloor,
439 which resulted from mass wasting processes involving blocks of gypsum and vuggy carbonate (Fig.
440 12B). As a consequence of partial dissolution of gypsum in seawater, dense brine is suggested to

have formed in depressions. Such conditions are known from deep sea hypersaline basins of the Eastern Mediterranean ridge (e.g. Camerlenghi, 1990), although at a larger scale than inferred for this study site. In such depressions filled with stagnant brines, anoxic conditions developed, hampering the life of infaunal metazoans. Vestimentiferan worms settled on morphological highs, allowing their tubes to project into an oxic water column. This way, vestimentiferans supposedly were able to take up oxygen and still benefit from methane seepage (Fig. 12B). The *Lucina* carbonates could only have formed where methane emission reached those parts of the seafloor placed well above the oxic-anoxic boundary in the water column, allowing them to mine sulphide from the anoxic sediment below (Fig. 12B). After their formation, *Lucina* and tubeworm carbonates were involved in mass wasting processes, responsible for the final emplacement within the VVCC succession at the end of the second MSC stage (Fig. 12C).

## 7. Conclusions

The authigenic carbonate rocks of the study area allow to reconstruct the evolution of a seepage system during the Messinian salinity crisis. The carbonates display features that result from hydrocarbon seepage into a sulphate-enriched body of water. Such sulphate enrichment resulted from both seawater evaporation (as reflected in the vuggy carbonates) and dissolution of gypsum deposits (*Lucina* and tubeworm carbonates). Although all studied rock types occur as blocks within a chaotic gravity flow deposit, their lithological features allow to establish a putative relative chronology of their formation and to relate them to different stages of the MSC. Vuggy carbonates are suggested to have formed during the first MSC stage under hypersaline conditions, agreeing with the apparent lack of chemosymbiotic communities caused by extreme environmental conditions. Tubeworm and *Lucina* carbonates likely formed during the second MSC stage under less severe conditions, allowing the survival of seep-dwelling metazoans. The fate of

vestimentiferan and bivalve communities is envisaged to have been controlled by the interaction of a rugged seafloor topography and dense anoxic brines, produced by the dissolution of gypsum.

**Acknowledgements**

We thank G. Carnevale for palaeontologic identification and A. Fusconi for help with UV microscopy, as well as the editor B. Teichert and two anonymous reviewers for helpful comments and suggestions. Financial support was provided by MIUR grant (Prin 2008) to D. Violanti and by IAS postgraduate grant to Marcello Natalicchio ($2^{nd}$ session, 2008).

**References**

Aloisi, G., Pierre, C., Rouchy, J.-M., Foucher, J.P., Woodside, J., Medinaut Scientific Party, 2000. Methane-related authigenic carbonates of eastern Mediterranean Sea mud volcanoes and their possible relation to gas hydrate destabilisation. Earth and Planetary Science Letters 184, 321-338.

Aloisi, G., Bouloubassi, I., Heijs, S.K., Pancost, R.D., Pierre, C., Sinninghe Damsté, J.S., Gottschal, J.C., Forney, L.J., Rouchy, J.-M., 2002. $CH_4$-consuming microorganisms and the formation of carbonate crusts at cold seeps. Earth and Planetary Science Letters 203, 195-203.

Amano, K., Jenkins, R.G., 2007. Eocene drill holes in cold-seep bivalves of Hokkaido, northern Japan. Marine Ecology 28, 108-114.

Arvidson, R.S., Morse, J.W., Joye, S.B., 2004. The sulfur biogeochemistry of chemosynthetic cold seep communities, Gulf of Mexico, USA. Marine Chemistry 87, 97-119.

Bertoni, C., Cartwright, J.A., 2007. Clastic depositional systems at the base of the late Miocene evaporites of the Levant region, Eastern Mediterranean. Geological Society, London, Special Publications 285, 37-52.

Bigi, G., Cosentino, D., Parotto, M., Sartori, R., Scandone, P., 1990. Structural Model of Italy: Geodinamic Project: Consiglio Nazionale delle Ricerche, S.EL.CA, scale 1:500,000, sheet 1.

Boetius, A., Ravenschlag, K., Schubert, C.J., Rickert, D., Widdel, F., Gieseke, A., Amann, R., Jørgensen, B.B., Witte, U., Pfannkuche, O., 2000. A marine microbial consortium apparently mediating anaerobic oxidation of methane. Nature 407, 623-626.

Camerlenghi, A., 1990. Anoxic basins of the eastern Mediterranean: geological framework. Marine Chemistry 31, 1-19.

Campbell, K.A., 2006. Hydrocarbon seep and hydrothermal vent paleoenvironments and paleontology: Past developments and future research directions. Palaeogeography, Palaeoclimatology, Palaeoecology 232, 362-407.

Cavagna, S., Clari, P., Martire, L., 1999. The role of bacteria in the formation of cold seep carbonates: geological evidence from Monferrato (Tertiary , NW Italy). Sedimentary Geology 126, 253-270.

CIESM, 2008. The Messinian Salinity Crisis from mega-deposits to microbiology – a consensus report. In: Briand, F., (Ed.), CIESM Workshop Monographs 33, Monaco, pp.168.

Clari, P.A., Gagliardi, C., Governa, M.E., Ricci, B., Zuppi, G.M., 1988. I Calcari di Marmorito: una testimonianza di processi diagenetici in presenza di metano. Bollettino del Museo Regionale di Scienze Naturali di Torino 5, 197-216.

Clari, P.A., Fornara, L., Ricci, B., Zuppi, G.M., 1994. Methane-derived carbonates and chemosymbiotic communities of Piedmont (Miocene), Northern Italy: an update. Geo-Marine Letters 14, 201-209.

Clari, P., Cavagna, S., Martire, L., Hunziker, J., 2004. A Miocene mud volcano and its plumbing system: A chaotic complex revisited (Monferrato, NW Italy). Journal of Sedimentary Research 74, 662-676.

Clari, P., Dela Pierre, F., Martire, L., Cavagna, S., 2009. The Cenozoic $CH_4$-derived carbonates of Monferrato (NW Italy): A solid evidence of fluid circulation in the sedimentary column. Marine Geology 265, 167-184.

Conti, S., Fontana, D., 2005. Anatomy of seep-carbonates: Ancient examples from the Miocene of the northern Apennines (Italy). Palaeogeography, Palaeoclimatology, Palaeoecology 227, 156-175.

Conti, S., Fontana, D., Lucente, C.C., 2008. Authigenic seep-carbonates cementing coarse-grained deposits in a fan-delta depositional system (middle Miocene, Marnoso-arenacea Formation, central Italy). Sedimentology 55, 471-486.

Cordes, E.E., Bergquist, D.C., Shea, K., Fisher, C.R., 2003. Hydrogen sulphide demand of long-lived vestimentiferan tube worm aggregations modifies the chemical environment at deep-sea hydrocarbon seeps. Ecology Letters 6, 212-219.

542

543 Cordes, E.E., Cunha, M.R., Galéron, J., Mora, C., Olu-Le Roy, K., Sibuet, M., Van Gaever, S.,
544 Vanreusel, A., Levin, L.A., 2010. The influence of geological, geochemical, and biogenic habitat
545 heterogeneity on seep biodiversity. Marine Ecology 31, 51-65.

546

547 Dattagupta, S., Miles, L.L., Barnabei, M.S., Fisher, C.R., 2006. The hydrocarbon seep tubeworm
548 *Lamellibrachia luymesi* primarily eliminates sulfate and hydrogen ions across its roots to conserve
549 energy and ensure sulfide supply. The Journal of Experimental Biology 209, 3795-3805.

550

551 Dattagupta, S., Arthur, M.A., Fisher, C.R., 2008. Modification of sediment geochemistry by
552 hydrocarbon seep tubeworm *Lamellibrachia luymesi*: a combined empirical and modeling
553 approach. Geochimica et Cosmochimica Acta 72, 2298–2315.

554

555 Dela Pierre, F., Festa, A., Irace, A., 2007. Interaction of tectonic, sedimentary and diapiric
556 processes in the origin of chaotic sediments: an example from the Messinian of Torino Hill
557 (Tertiary Piedmont Basin, northwestern Italy). Geological Society of America Bulletin 119, 1107-
558 1119.

559

560 Dela Pierre, F., Martire, L., Natalicchio, M., Clari, P.A., Petrea, C., 2010. Authigenic carbonates in
561 the upper Miocene sediments of the Tertiary Piedmont Basin (NW Italy): vestiges of an ancient gas
562 hydrate stability zone. Geological Society of America Bulletin 122, 994-1010.

563

564 Dela Pierre, F., Bernardi, E., Cavagna, S., Clari, P., Gennari, R., Irace, A., Lozar, F., Lugli, S.,
565 Manzi, V., Natalicchio, M., Roveri, M., Violanti, D., 2011. The record of the Messinian salinity
566 crisis in the Tertiary Piedmont Basin (NW Italy): The Alba section revisited. Palaeogeography,
567 Palaeoclimatology, Palaeoecology 310, 238-255.

568

569 Dela Pierre, F., Clari, P., Bernardi, E., Natalicchio, M., Costa, E., Cavagna, S., Lozar, F., Lugli, S.,
570 Manzi, V., Roveri, M., Violanti, D., 2012. Messinian carbonate-rich beds of the Tertiary Piedmont
571 Basin (NW Italy): Microbially-mediated products straddling the onset of the salinity crisis.
572 Palaeogeography, Palaeoclimatology, Palaeoecology 344-345, 78-93.

573

574 Djamali, M., Ponel, P., Delille, T., Thiéry, A., Asem, A., Andrieu-Ponel, V., de Beaulieu, J.-L.,
575 Lahijani, H., Shah-Hosseini, M., Amini, A., Stevens, L., 2010. A 200,000-year record of the brine
576 shrimp *Artemia* (Crustacea: Anostraca) remains in Lake Urmia , NW Iran. International Journal of
577 Aquatic Science 1, 14-18.

578

579 Duperron, S., Nadalig, T., Caprais, J.-C., Sibuet, M., Fiala-Médioni, A., Amann, R., Dubilier, N.,
580 2005. Dual symbiosis in a *Bathymodiolus* sp. mussel from a methane seep on the Gabon continental
581 margin (Southeast Atlantic): 16S rRNA phylogeny and distribution of the symbionts in gills.
582 Applied and Environmental Microbiology 71, 1694–1700.

583

584 Freytag, J.K., Girguis, P.R., Bergquist, D.C., Andras, J.P., Childress, J.J., Fisher, C.R., 2001. A
585 paradox resolved: sulfide acquisition by roots of seep tubeworms sustains net chemoautotrophy.
586 Proceedings of the National Academy of Sciences of the United States of America 98, 13408-
587 13413.

588

589 Ghibaudo, G., Clari, P., Perello, M., 1985. Litostratigrafia, sedimentologia ed evoluzione tettonico-
590 sedimentaria dei depositi miocenici del margine sud-orientale del Bacino Terziario Ligure-
591 Piemontese (valli Borbera, Scrivia e Lemme). Bollettino della Società Geologica Italiana 104, 349-
592 397.

Goedert, J.L., Peckmann, J., Reitner, J., 2000. Worm tubes in allochthonous cold-seep carbonates from Lower Oligocene rocks of western Washington. Journal of Paleontology 74, 992–999.

Gorini, C., Lofi, J., Duvail, C., Dosreis, a, Guennoc, P., Lestrat, P., Mauffret, A., 2005. The Late Messinian salinity crisis and Late Miocene tectonism: Interaction and consequences on the physiography and post-rift evolution of the Gulf of Lions margin. Marine and Petroleum Geology 22, 695-712.

Guido, A., Jacob, J., Gautret, P., Laggoun-Défarge, F., Mastandrea, A., Russo, F., 2007. Molecular fossils and other organic markers as palaeoenvironmental indicators of the Messinian Calcare di Base Formation: normal versus stressed marine deposition (Rossano Basin, northern Calabria, Italy). Palaeogeography, Palaeoclimatology, Palaeoecology 255, 265-283.

Haas, A., Little, C.T.S., Sahling, H., Bohrmann, G., Himmler, T., Peckmann, J., 2009. Mineralization of vestimentiferan tubes at methane seeps on the Congo deep-sea fan. Deep-Sea Research Part I: Oceanographic Research Papers 56, 283-293.

Hammer, Ø., Nakrem, H.A., Little, C.T.S., Hryniewicz, K., Sandy, M.R., Hurum, J.H., Druckenmiller, P., Knutsen, E.M., Høyberget, M., 2011. Hydrocarbon seeps from close to the Jurassic–Cretaceous boundary, Svalbard. Palaeogeography, Palaeoclimatology, Palaeoecology 306, 15-26.

Himmler, T., Freiwald, A., Stollhofen, H., Peckmann, J., 2008. Late Carboniferous hydrocarbon-seep carbonates from the glaciomarine Dwyka Group, southern Namibia. Palaeogeography, Palaeoclimatology, Palaeoecology 257, 185-197.

Hsü, K.J., Cita, M.B., Ryan, W.B.F., 1973. The origin of the Mediterranean evaporites. In: Ryan, W.B.F., Hsü, K.J., et al. (Eds.), Initial Report of Deep Sea Drilling Program 13. U.S. Government Printing Office, Washington DC, pp. 1203–1231.

Julian, D., Gaill, F., Wood, E., Arp, A.J., Fisher, C.R., 1999. Roots as a site of hydrogen sulfide uptake in the hydrocarbon seep vestimentiferan *Lamellibrachia* sp. The Journal of Experimental Biology 202, 2245-2257.

Kelley, P., Hansen, T.A., 2003. The fossil record of drilling predation on bivalves and gastropods. In: Kelley, P., Kowalewski, M., Hansen, T.A. (Eds), Predator-Prey Interactions in the Fossil Record. Kluwer Academic Plenum Publishers, New York, pp. 113-139.

Kiel, S., Dando, P.R., 2009. Chaetopterid tubes from vent and seep sites: Implications for the fossil record and evolutionary history of vent and seep annelids. Acta Palaeontologica Polonica 54, 443-448

Levin, L.A., 2005. Ecology of cold seep sediments: interactions of fauna with flow, chemistry and microbes. Oceanography and Marine Biology: An Annual Review 43, 1-46.

Lofi, J., Gorini, C., Berne, S., Clauzon, G., Tadeudosreis, A., Ryan, W., Steckler, M., 2005. Erosional processes and paleo-environmental changes in the Western Gulf of Lions (SW France) during the Messinian Salinity Crisis. Marine Geology 217, 1-30.

642

643 Manzi, V., Lugli, S., Lucchi, F.R., Roveri, M., 2005. Deep-water clastic evaporites deposition in the
644 Messinian Adriatic foredeep (northern Apennines, Italy): did the Mediterranean ever dry out?
645 Sedimentology 52, 875-902.

646

647 Manzi, V., Roveri, M., Gennari, R., Bertini, A., Biffi, U., Giunta, S., Iaccarino, S.M., Lanci, L.,
648 Lugli, S., Negri, A., 2007. The deep-water counterpart of the Messinian Lower Evaporites in the
649 Apennine foredeep: The Fanantello section (Northern Apennines, Italy). Palaeogeography,
650 Palaeoclimatology, Palaeoecology 251, 470-499.

651

652 Manzi, V., Lugli, S., Roveri, M., Schreiber, B.C., Gennari, R., 2011. The Messinian "Calcare di
653 Base" (Sicily, Italy) revisited. Geological Society of America Bulletin 123, 347-370.

654

655 Mazzini, A., Jonk, R., Duranti, D., Parnell, J., Cronin, B., Hurst, A., 2003. Fluid escape from
656 reservoirs: implications from cold seeps, fractures and injected sands Part I. The fluid flow system.
657 Journal of Geochemical Exploration 78-79, 293-296.

658

659 Mazzini, A., Ivanov, M., Nermoen, A., Bahr, A., Bohrmann, G., Svensen, H., Planke, S., 2008.
660 Complex plumbing systems in the near subsurface: Geometries of authigenic carbonates from
661 Dolgovskoy Mound (Black Sea) constrained by analogue experiments. Marine and Petroleum
662 Geology 25, 457-472.

663

664 McCrea, J.M., 1950. On the isotopic chemistry of carbonates and a paleotemperature scale. Journal
665 of Chemical Physics 18, 849-857.

666

667 Mosca, P., Polino, R., Rogledi, S., Rossi, M., 2009. New data for the kinematic interpretation of the
668 Alps–Apennines junction (Northwestern Italy). International Journal of Earth Sciences 99, 833-849.
669
670 Natalicchio, M., Birgel, D., Dela Pierre, F., Martire, L., Clari, P., Spötl, C., Peckmann, J., 2012.
671 Polyphasic carbonate precipitation in the shallow subsurface: Insights from microbially-formed
672 authigenic carbonate beds in upper Miocene sediments of the Tertiary Piedmont Basin (NW Italy).
673 Palaeogeography, Palaeoclimatology, Palaeoecology 329-330, 158-172.
674
675 Oliveri, E., Neri, R., Bellanca, A., Riding, R., 2010. Carbonate stromatolites from a Messinian
676 hypersaline setting in the Caltanissetta Basin, Sicily: petrographic evidence of microbial activity
677 and related stable isotope and rare earth element signatures. Sedimentology 57, 142-161.
678
679 Olu-Le Roy, K., Caprais, J.-C., Fifis, A., Fabri, M.C., Galéron, J., Budzinsky, H., Le Ménach, K.,
680 Khripounoff, A., Ondréas, H., Sibuet, M., 2007. Cold-seep assemblages on a giant pockmark off
681 West Africa: spatial patterns and environmental control. Marine Ecology 28, 115-130.
682
683 Orphan, V.J., House, C.H., Hinrichs, K.-U., McKeegan, K.D., Delong E.F., 2002. Multiple archaeal
684 groups mediate methane oxidation in anoxic cold seep sediments. Proceedings of the National
685 Academy of Sciences USA 99, 7663-7668.
686
687 Orszag-Sperber, F., 2006. Changing perspectives in the concept of "Lago-Mare" in Mediterranean
688 Late Miocene evolution. Sedimentary Geology 188-189, 259-277.
689
690 Paull, C.K., Chanton, J.P., Neumann, A.C., Coston, J.A., Martens, C.S., Showers, W., 1992.
691 Indicators of methane-derived carbonates and chemosynthetic organic carbon deposits; examples
692 from the Florida Escarpment. Palaios 7, 361-375.

693

694 Peckmann, J., Thiel, V., 2004. Carbon cycling at ancient methane–seeps. Chemical Geology 205,
695 443-467.

696

697 Peckmann, J., Thiel, V., Michaelis, W., Clari, P., Gaillard, C., Martire, L., Reitner, J., 1999. Cold
698 seep deposits of Beauvoisin (Oxfordian; southeastern France) and Marmorito (Miocene; northern
699 Italy): microbially induced authigenic carbonates. International Journal of Earth Sciences 88, 60-75.

700

701 Peckmann, J., Goedert, J.L., Thiel, V., Michaelis, W., Reitner, J., 2002. A comprehensive approach
702 to the study of methane-seep deposits from the Lincoln Creek Formation, western Washington
703 State, USA. Sedimentology 49, 855-873.

704

705 Peckmann, J., Thiel, V., Reitner, J., Taviani, M., Aharon, P., Michaelis, W., 2004. A microbial mat
706 of a large sulfur bacterium preserved in a Miocene methane-seep limestone. Geomicrobiology
707 Journal 21, 247-255.

708

709 Peckmann, J., Little, C.T.S., Gill, F., Reitner, J., 2005. Worm tube fossils from the Hollard Mound
710 hydrocarbon-seep deposit, Middle Devonian, Morocco: Palaeozoic seep-related vestimentiferans?
711 Palaeogeography, Palaeoclimatology, Palaeoecology 227, 242-257.

712

713 Peckmann, J., Kiel, S., Sandy, M.R., Taylor, D.G., Goedert, J.L., 2011. Mass occurrences of
714 the brachiopod *Halorella* in Late Triassic methane-seep deposits, eastern Oregon. Journal of
715 Geology 119, 207–220.

716

717 Ricci Lucchi, F., Vai, G.B., 1994. A stratigraphic and tectonofacies framework of the “calcari a
718 *Lucina*” in the Apennine Chain, Italy. Geo-Marine Letters 14, 210-218.

719

720 Riding, R., 2000. Microbial carbonates: the geological record of calcified bacterial–algal mats and
721 biofilms. Sedimentology 47, 179-214.

722

723 Ritger, S., Carson, B., Suess, E., 1987. Methane-derived authigenic carbonates formed by
724 subduction- induced pore-water expulsion along the Oregon/Washington margin. Geological
725 Society of America Bulletin 98, 147-156.

726

727 Roberts, H.H., Aharon, P., 1994. Hydrocarbon-derived carbonate buildups of the northern Gulf of
728 Mexico continental slope: a review of submersible investigations. Geo-Marine Letters 14, 135-148.

729

730 Roberts, H.H., Feng, D., Joye, S.B., 2010. Cold-seep carbonates of the middle and lower
731 continental slope, northern Gulf of Mexico. Deep-Sea Research Part II 57, 2040–2054.

732

733 Rouchy, J., Caruso, A., 2006. The Messinian salinity crisis in the Mediterranean basin: A
734 reassessment of the data and an integrated scenario. Sedimentary Geology 188-189, 35-67.

735

736 Roveri, M., Lugli, S., Manzi, V., Schreiber, B.C., 2008. The Messinian Sicilian stratigraphy
737 revisited: new insights for the Messinian salinity crisis. Terra Nova 20, 483-488.

738

739 Sahling, H., Bohrmann, G., Spiess, V., Bialas, J., Breitzke, M., Ivanov, M., Kasten, S., Krastel, S.,
740 Schneider, R., 2008. Pockmarks in the Northern Congo Fan area, SW Africa: Complex seafloor
741 features shaped by fluid flow. Marine Geology 249, 206-225.

742

743 Sass, E., Bein, A., Almogi-Labin, A., 1991. Oxygen-isotope composition of diagenetic calcite in
744 organic-rich rocks: evidence for $^{18}O$ depletion in marine anaerobic pore water. Geology 19, 839-
745 842.

746

747 Schreiber, B.C., Friedman, G.M., Decima, A. and Schreiber, E., 1976. The depositional
748 environments of the Upper Miocene (Messinian) evaporite deposits of the Sicilian Basin.
749 Sedimentology 23, 729-760.

750

751 Taviani, M., 1994. The "calcari a *Lucina*" macrofauna reconsidered: Deep-sea faunal oases from
752 Miocene-age cold vents in the Romagna Apennine, Italy. Geo-Marine Letters 14, 185-191.

753

754 Taviani, M., 2001. Fluid venting and associated processes. In: Vai, G.B., Martini, P. (Eds.),
755 Anatomy of a mountain: the Apennines and adjacent Mediterranean, Kluwer Academic Publishers,
756 pp. 351-366.

757

758 Taviani, M., 2011. The deep-sea chemoautotroph microbial world as experienced by the
759 Mediterranean metazoans through time. In: Reitner, J., Quéric, N.V., Arp, G., (Eds.),
760 Advances in Stromatolite Geobiology, Lecture Notes in Earth Sciences 131, Springer-Verlag, pp.
761 277-295.

762

763 Taylor, J.D., Glover, E.A., 2009. A giant lucinid bivalve from the Eocene of Jamaica − Systematics,
764 life habits and chemosymbiosis (Mollusca: Bivalvia: Lucinidae). Palaeontology 52, 95-109,

765

766 Turchyn A.V., Brüchert, V., Lyons, T.W., Engel, G.S., Balci, N., Schrag, D.P, Brunner, B., 2010.
767 Kinetic oxygen isotope effects during dissimilatory sulfate reduction: A combined theoretical and
768 experimental approach. Geochimica et Cosmochimica Acta 74, 2011-2024.
769
770 Vasconcelos, C., McKenzie, J.A., Bernasconi, S., Grujic, D., Tien, A.J., 1995. Microbial mediation
771 as a possible mechanism for natural dolomite formation at low temperatures. Nature 377, 220-222.
772
773 Venturini, S., Selmo, E., Tarlao A., Tunis, G., 1998. Fossiliferous methanogenic limestones in the
774 Eocene flysch of Istria (Croatia). Giornale di Geologia 60, 219-234.
775
776 Warthmann, R., Lith, Y.V., Vasconcelos, C., McKenzie, J.A., Marie, A., 2000. Bacterially induced
777 dolomite precipitation in anoxic culture experiments, Geology 28, 1091-1094.
778
779 Ziegenbalg, S.B., Brunner, B., Rouchy, J.M., Birgel, D., Pierre, C., Böttcher, M.E., Caruso, A.,
780 Immenhauser, A., Peckmann, J., 2010. Formation of secondary carbonates and native sulphur in
781 sulphate-rich Messinian strata, Sicily. Sedimentary Geology 227, 37-50.
782
783 Ziegenbalg, S.B., Birgel, D., Hoffmann-Sell, L., Pierre, C., Rouchy, J.M., Peckmann, J., 2012.
784 Anaerobic oxidation of methane in hypersaline Messinian environments revealed by $^{13}$C-depleted
785 molecular fossils: Chemical Geology, 292-293, 140-148.

## FIGURE CAPTIONS

**Fig. 1** (A) Structural sketch map of northwestern Italy (modified from Bigi et al., 1990). (B) Schematic geological map of the study area showing the distribution of the main blocks of authigenic carbonate within the Valle Versa Chaotic Complex.

**Fig. 2** Correlation of the studied section (right) with the Messinian salinity crisis chronostratigraphic framework (modified from CIESM, 2008). The three intervals distinguished in the Valle Versa Chaotic Complex are indicated (*a*, *b*, and *c*). PLG: Primary Lower Gypsum; UG: Upper Gypsum; RLG: Resedimented Lower Gypsum; MES: Messinian Erosional Surface; SAF: Sant'Agata Fossili Marls; CSC: Cassano Spinola Conglomerates; VC: vuggy carbonates; LC: *Lucina* carbonates; TC: tubeworm carbonates. Note that in the Sant'Agata Fossili Marls in situ *Lucina* carbonates (LC) are also present. The 'v' symbols in the lithostratigraphic column indicate gypsum.

**Fig. 3** Outcrop view showing the erosional boundary (MES = Messinian erosional surface) separating the Sant'Agata Fossili Marls and the Valle Versa Chaotic Complex (VVCC). Note the two lowermost intervals of the VVCC (*a* and *b*) composed of selenite gypsum blocks.

**Fig. 4** (A) Outcrop view of the vuggy carbonates (VC); the dashed line indicates the sharp contact with laminated siltstone (Ss) containing remains of euryhaline fishes, including *Aphanius crassicaudus* (B). (C) Polished slab of the vuggy carbonates (sample CVP8); note the centimetre-sized cavities filled with micritic sediments (Sd) and polyphasic carbonate cements (Cm), floating within grey siltstone (Ss); carbon and oxygen isotope values of carbonate phases are shown.

**Fig. 5** (A) Vuggy carbonates composed of cemented silty-mudstones (Ss) and cavities filled with polyphasic carbonate cements (Cm) and sediments (Sed); plane-polarized light. Note the

812 pseudomorphs after gypsum partially filled with sediments (white arrow). (B) Detail of (A) showing
813 cluster of filaments; plane-polarized light. (C) Carbonate pseudomorphs after gypsum, crosscut by a
814 fracture filled with polyphasic carbonate cements; the isotope values of the fracture-filling cements
815 are indicated; plane-polarized light. (D) SEM image showing spheroidal dolomite crystals making
816 up the intergranular cement; note the central hollow of some dolomite crystals.
817
818 **Fig. 6** Outcrop view of *Lucina* carbonates.
819
820 **Fig. 7** (A) Outcrop view of tubeworm carbonates. (B) Detail of (A) showing centimetre-sized
821 angular clasts. (C) Close up of (A) showing a cluster of curved tubular structures. (D) Polished slab
822 of the tubular structures; note acicular aragonite (Ar) and minor sediments (Sed) filling the tubes.
823
824 **Fig. 8** Photomicrographs of tubeworm carbonates. (A) and (B) Tubes in cross section; note in (B)
825 aragonite needles on both the internal and external surface of the tube wall; plane-polarized light.
826 (C) and (D) Close up of tube walls; note the delamination of individual layers of the tube wall;
827 plane-polarized and fluorescent light, respectively. (D) Delaminated carbonate layers exhibit an
828 intense autofluorescence. (E) and (F) SEM views of tube wall; slightly etched, polished rock
829 surfaces; note carbonate pillars connecting two otherwise separated layers of the tube wall (arrows).
830
831 **Fig. 9 (A)** Tube infilled by clotted micrite and carbonate cement; plane-polarized light. (B)
832 Dolomite microspherulite coating the tube wall; note the dumbbell morphology of the central
833 hollow. (C) and (D) Detail of (A) showing irregular elongated rods (white arrows) and dolomite
834 microspherulites (black arrows); plane-polarized and fluorescent light, respectively. (D) Rods
835 (white arrows) reveal an intense autofluorescence.
836
837 **Fig. 10** Cross-plot of the stable isotope data.

838

839 **Fig. 11** Evolutionary stages envisaged for the genesis of vuggy carbonates; AOM = anaerobic
840 oxidation of methane; for further details see text.

841

842 **Fig. 12** Evolution of hydrocarbon seepage during the Messinian salinity crisis. (A) Formation of the
843 vuggy carbonates during the first MSC stage. Note that the stratigraphic relationship between vuggy
844 carbonates and gypsum are not longer preserved (see text). (B) Formation of tubeworm and *Lucina*
845 carbonates in the second MSC stage; OAb = oxic-anoxic boundary. (C) Final configuration after
846 carbonates have been involved in gravitative processes at the end of the second MSC stage.
847 Symbols and abbreviations are the same as in Fig. 2.

848

849

850 **TABLES**

851

852 **Table 1** Mineralogy, carbon and oxygen isotope composition of carbonate phases.

Figure1

Click here to download high resolution image

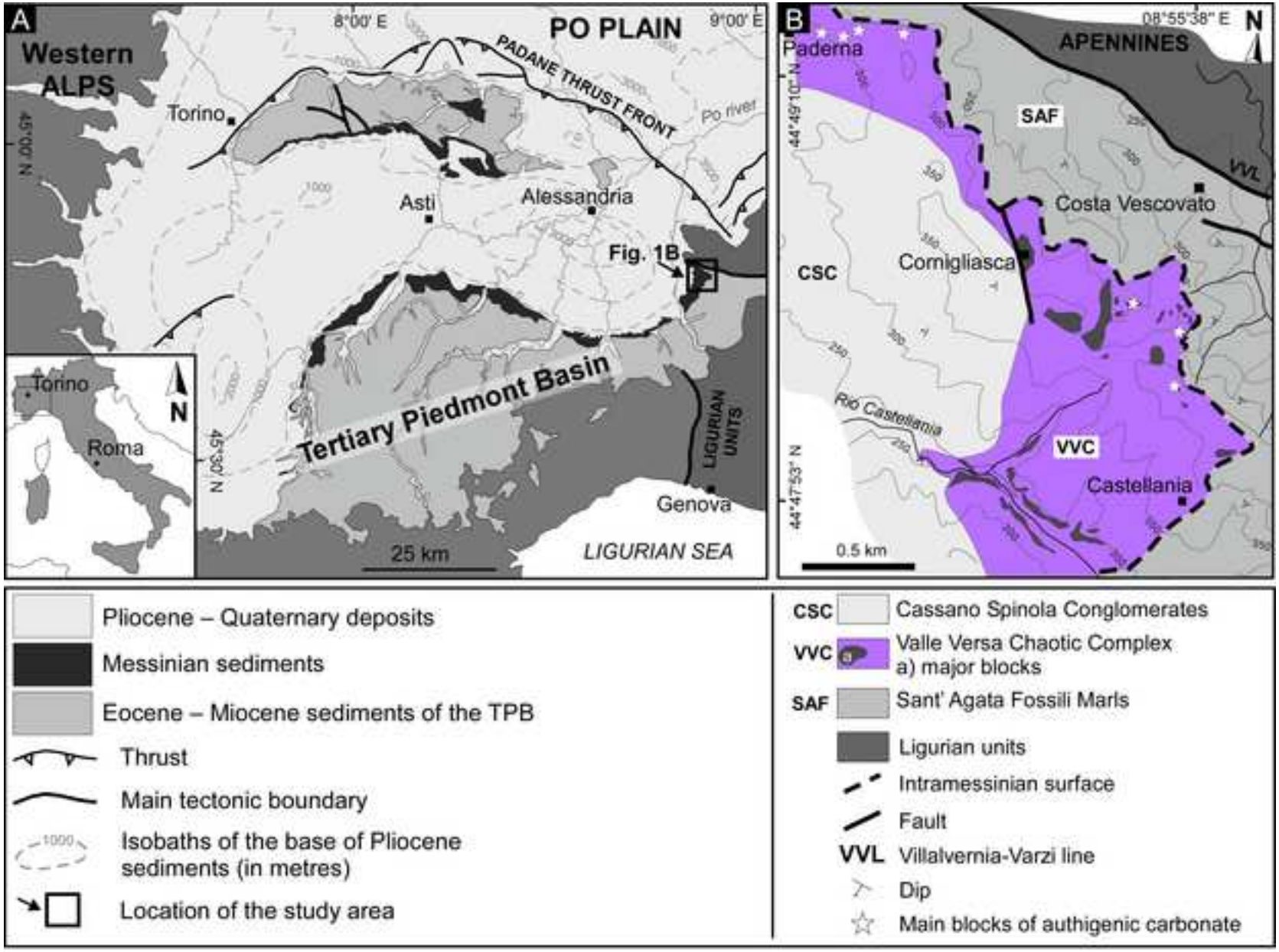


Natalicchio et al. Figure 1

Figure2

Click here to download high resolution image

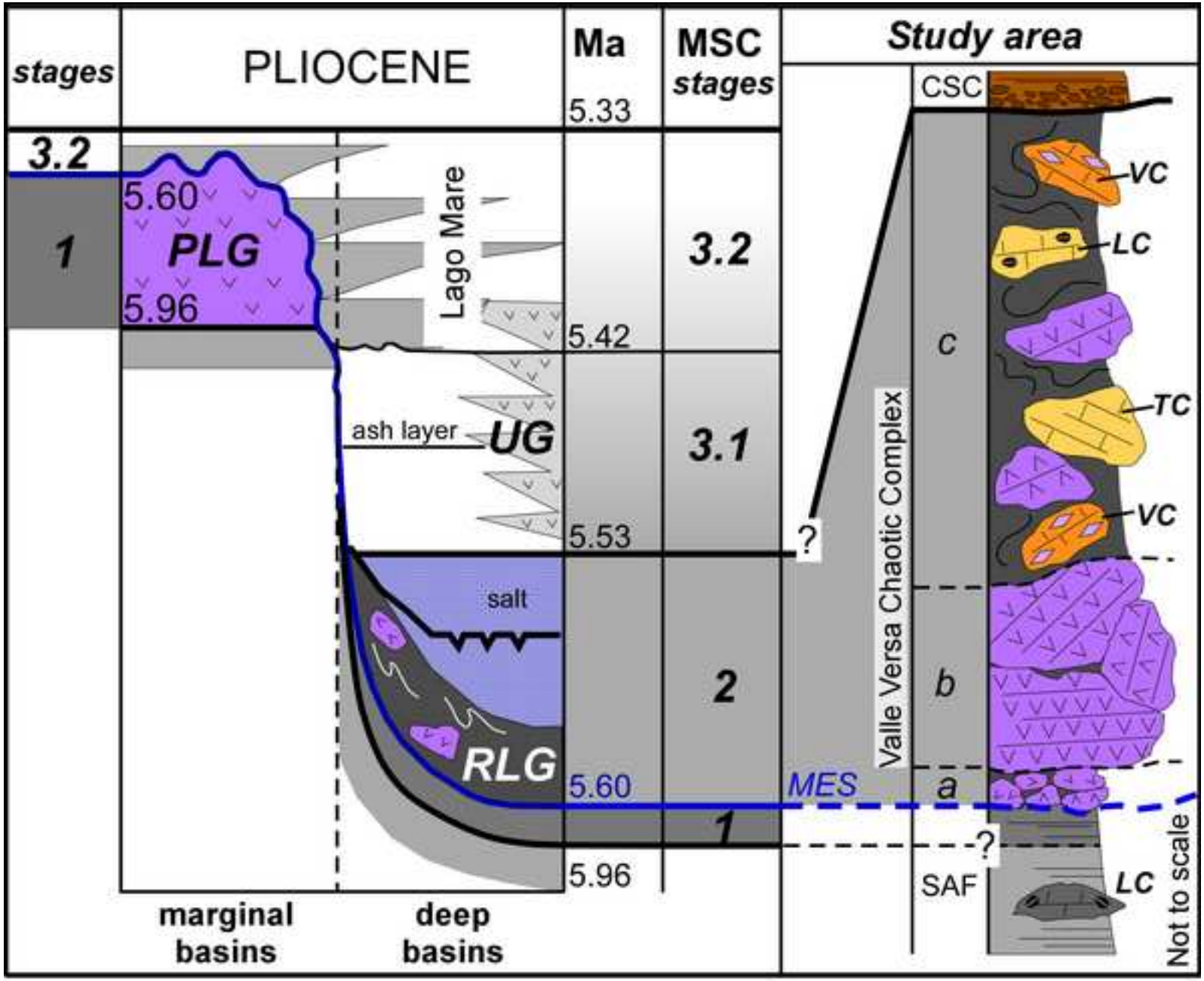


Natalicchio et al., Figure 2

Figure3
Click here to download high resolution image


Natalicchio et al., Figure 3

Figure4
Click here to download high resolution image

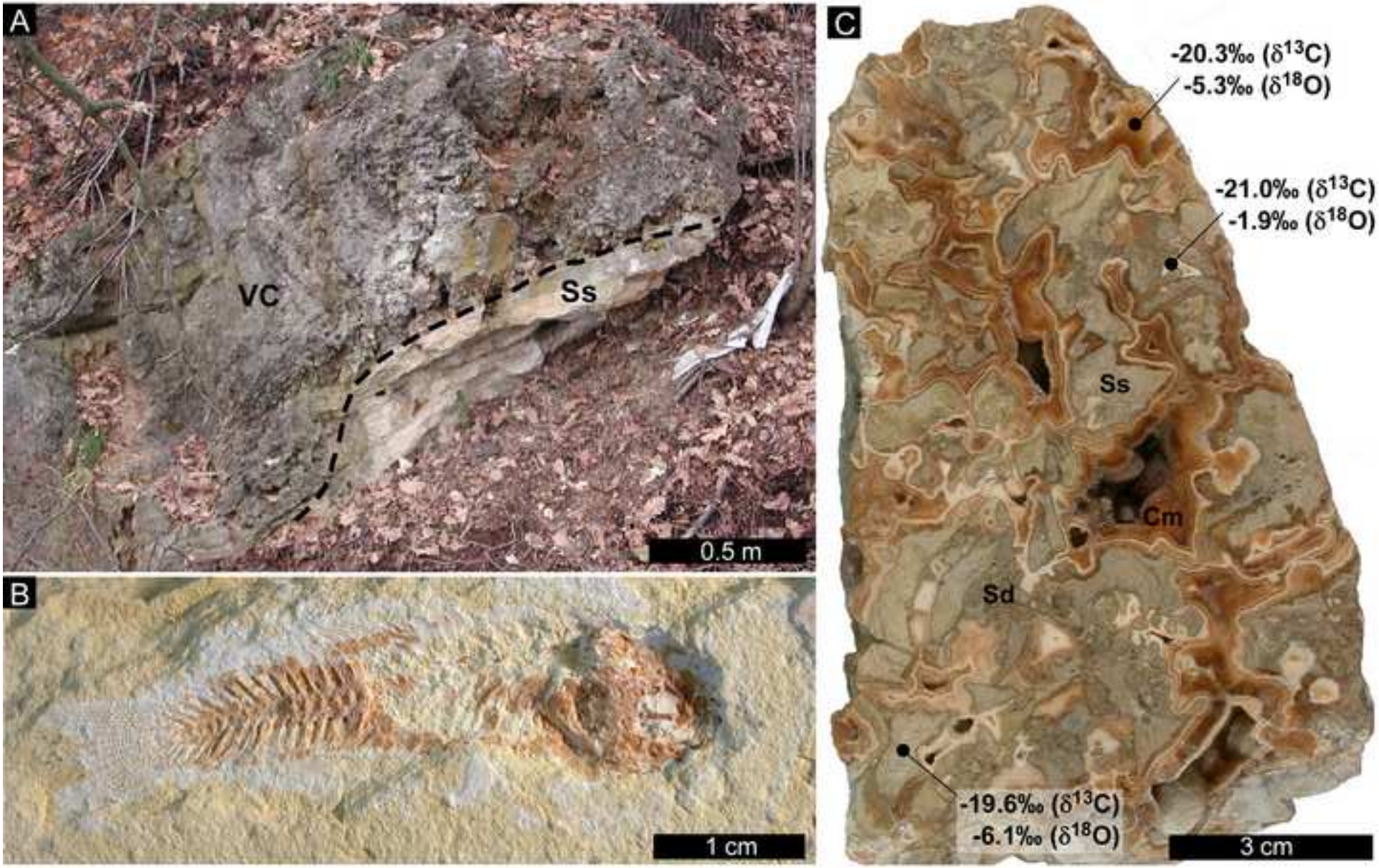


Natalicchio et al., Figure 4

Figure5

Click here to download high resolution image

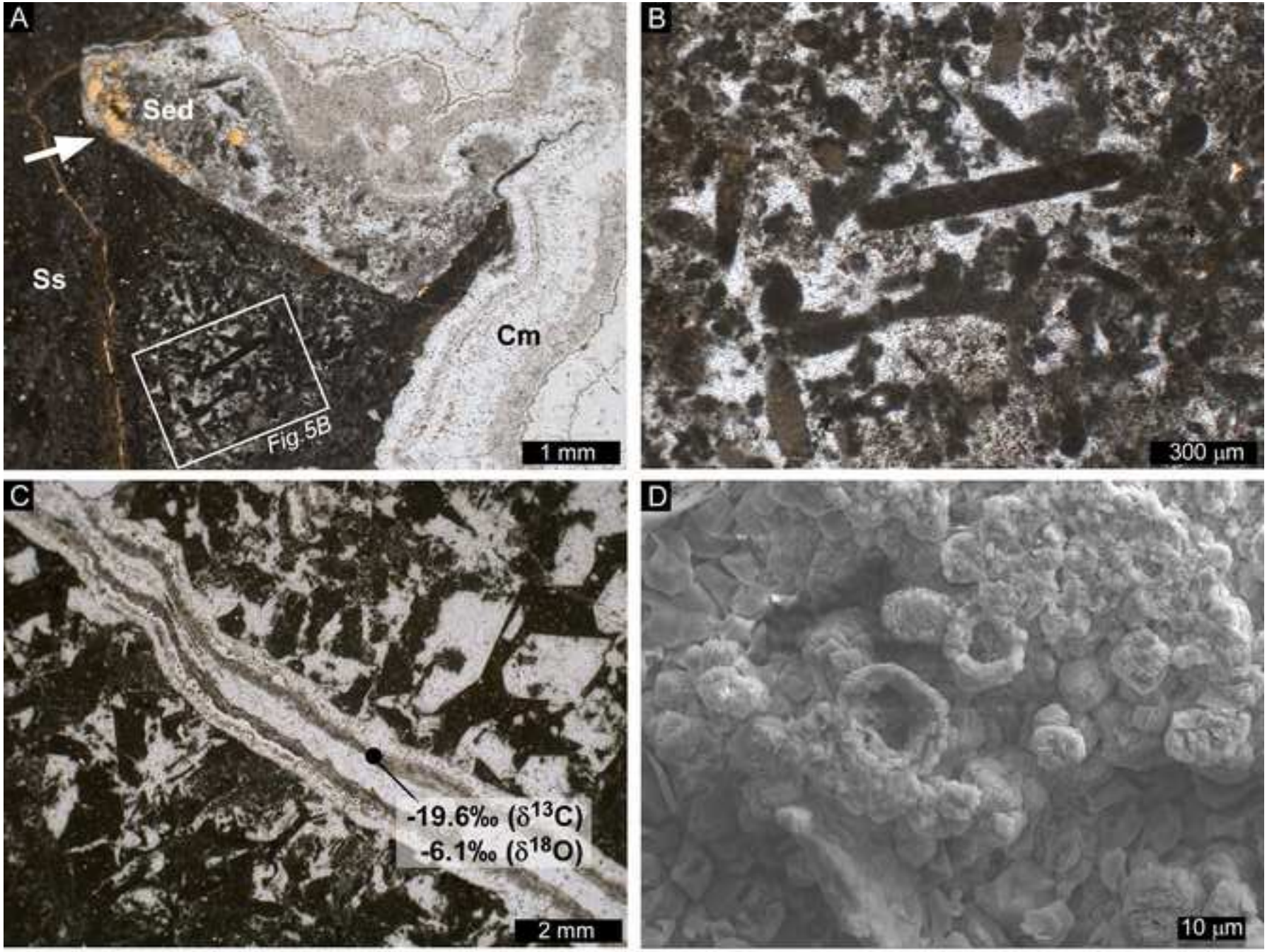


Natalicchio et al., Figure 5

Figure6

Click here to download high resolution image


Natalicchio et al., Fig. 6

Figure7

Click here to download high resolution image

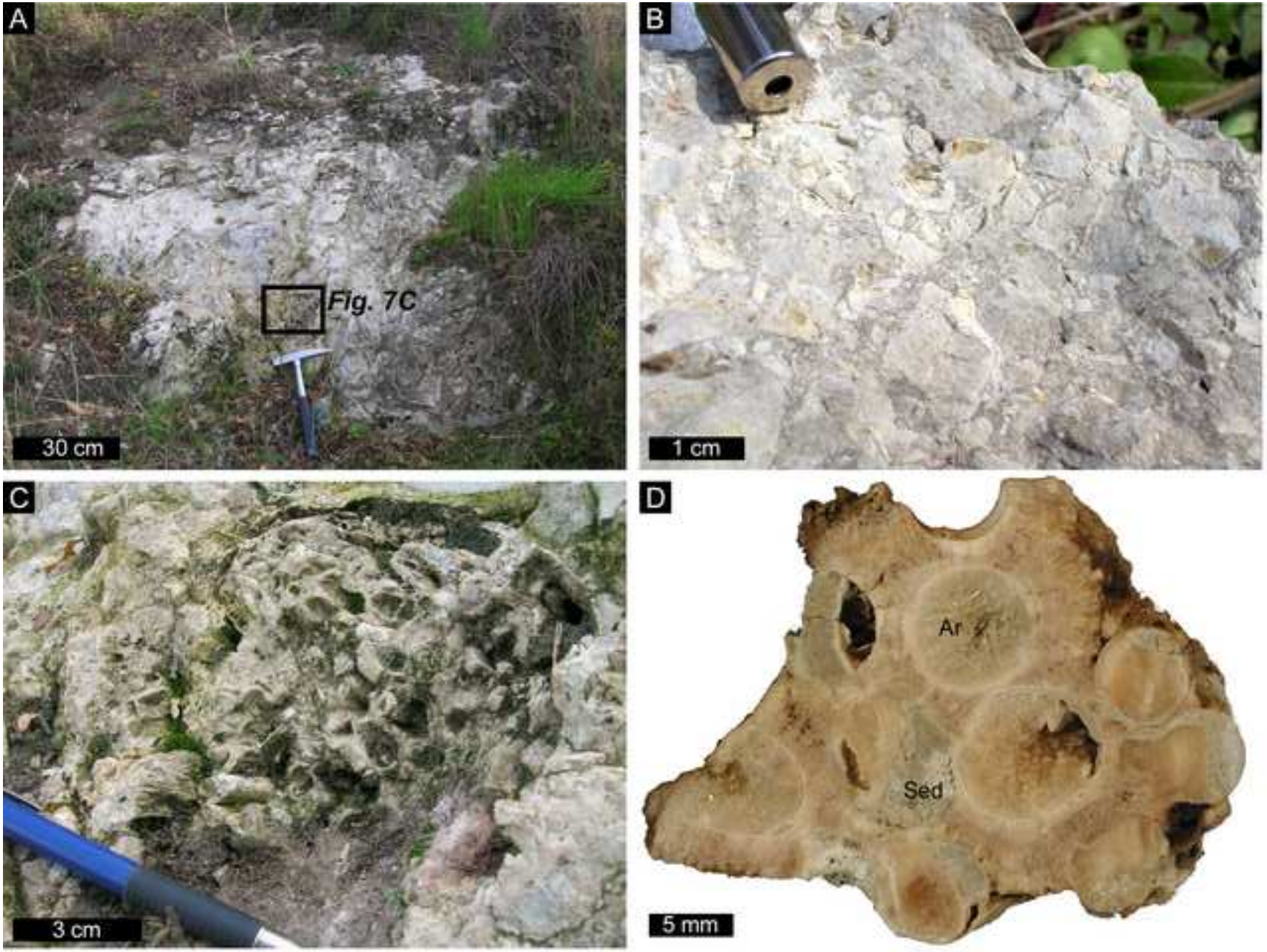


Natalicchio et al., Figure 7

**Figure8**

**Click here to download high resolution image**

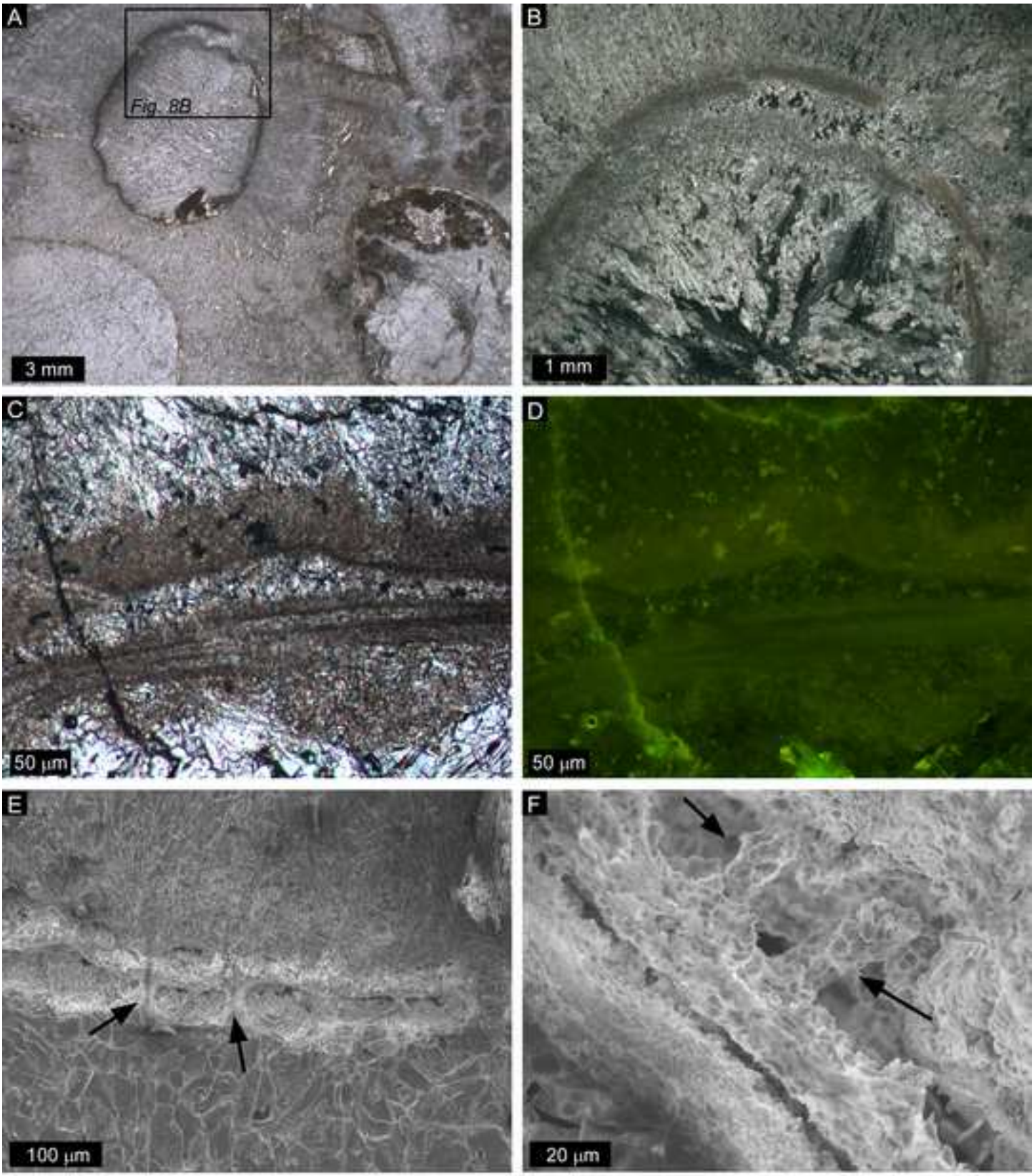


Natalicchio et al., Figure 8

Figure9

Click here to download high resolution image

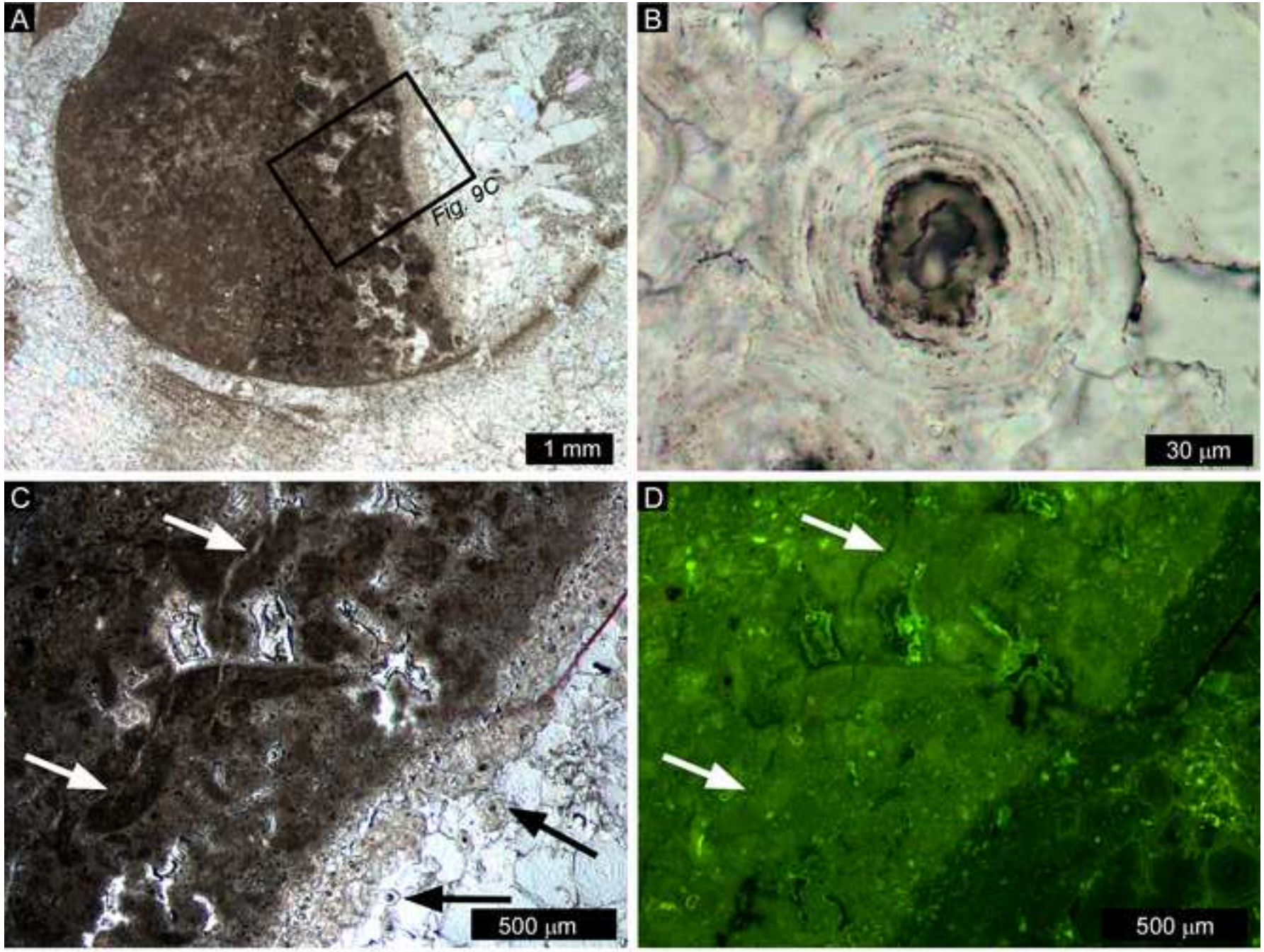


Natalicchio et al., Figure 9

Figure10
Click here to download high resolution image

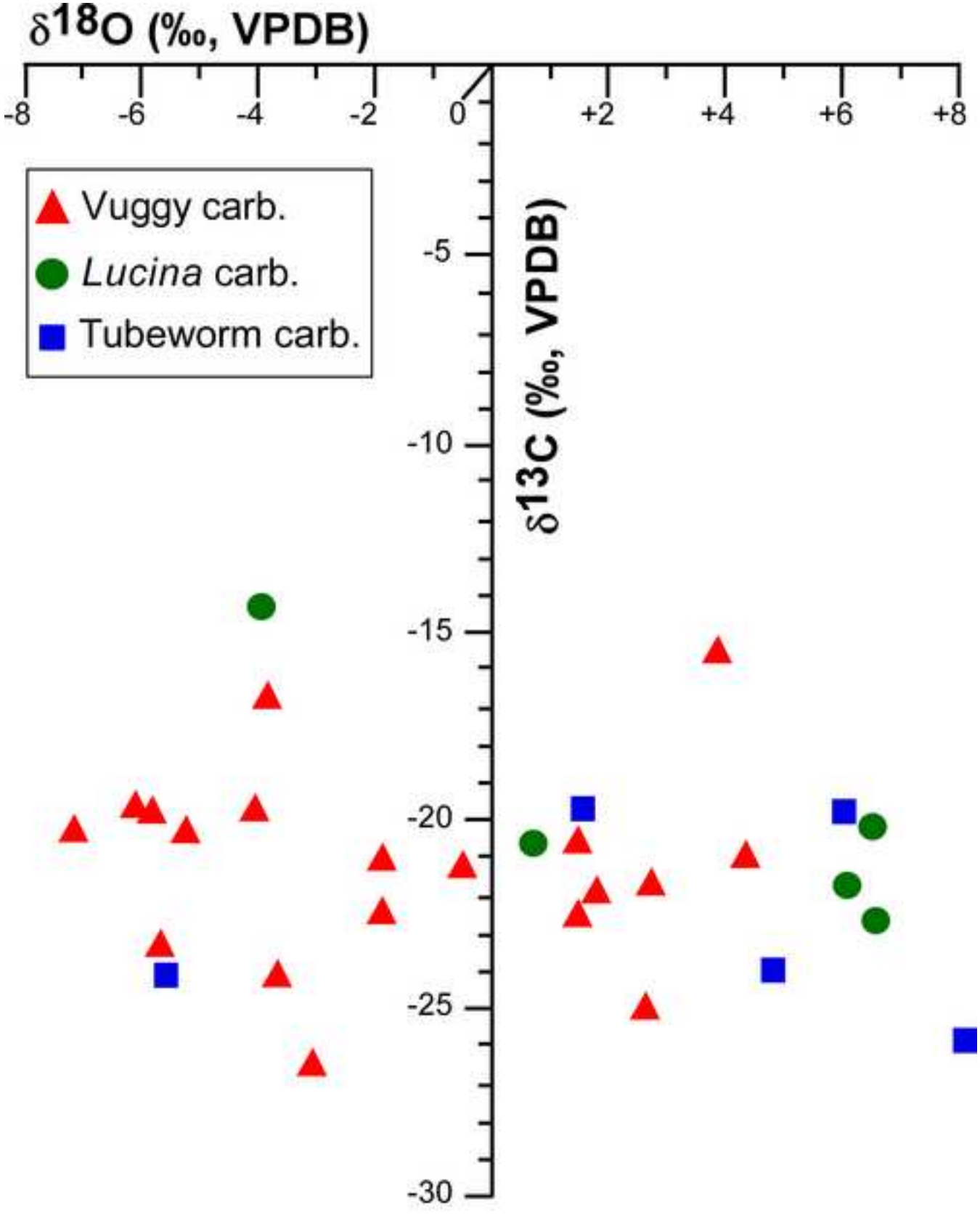


Natalicchio et al., Figure 10

Figure11

Click here to download high resolution image

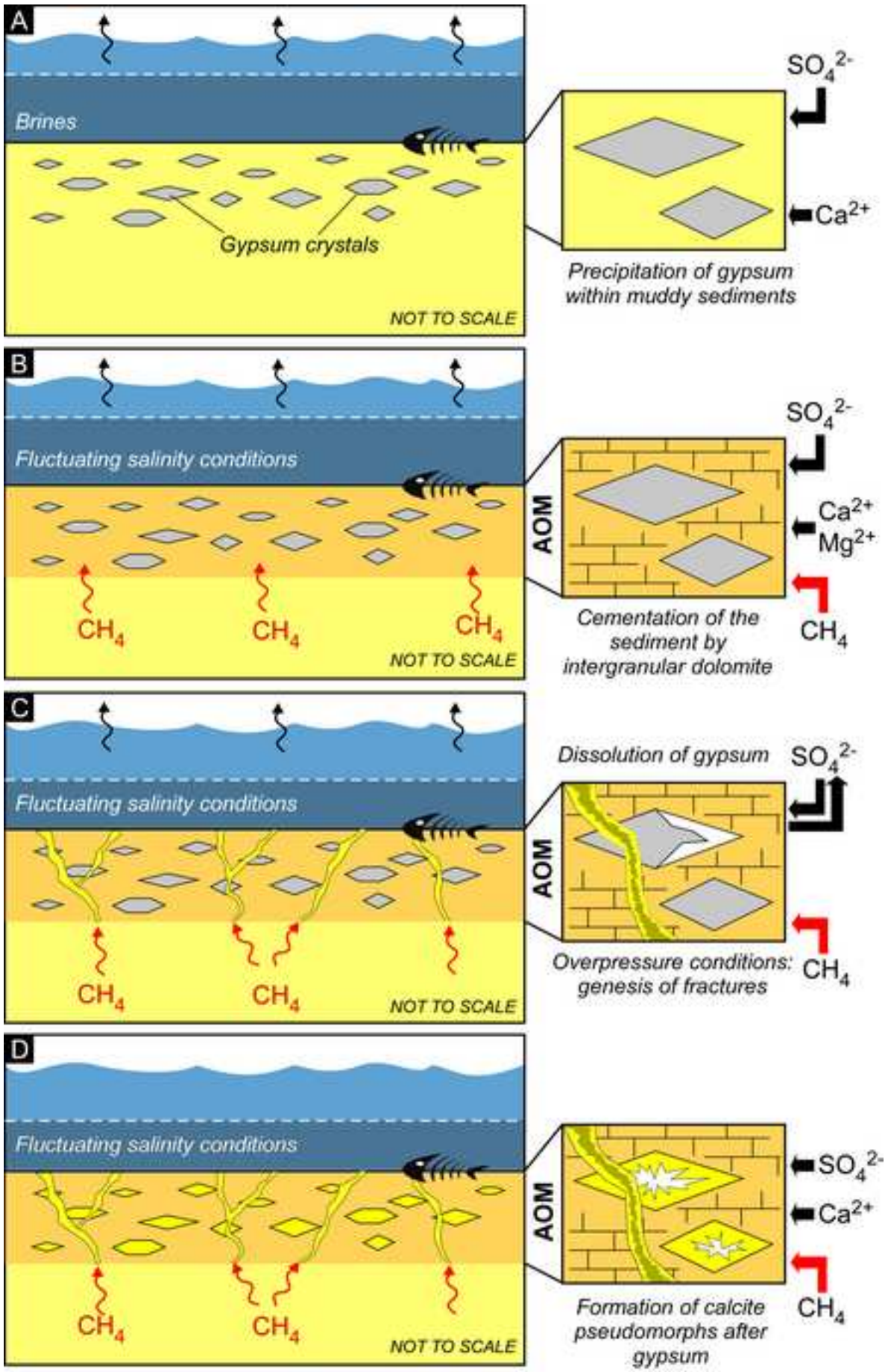


Natalicchio et al., Figure 11

Figure12
Click here to download high resolution image

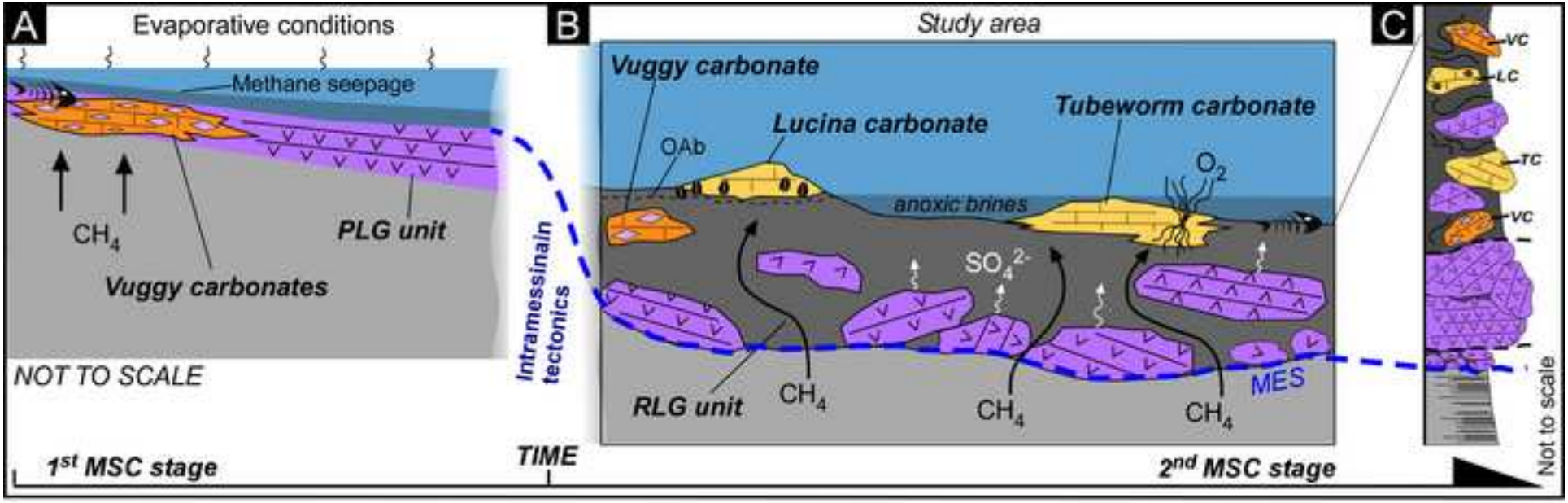


Natalicchio et al., Figure 12

**Table1**

**Click here to download Table: tab1_Natalicchio et al.doc**

| Sample | Mineralogy | Cement type | $\delta^{13}C$ [‰] | $\delta^{18}O$ [‰] |
|---|---|---|---|---|
| *Vuggy carbonates* | | | | |
| CVP8-1 4.2 | Calcite | Cavity-filling | −21.7 | +2.7 |
| CVP8-1 4.3 | Calcite | Cavity-filling | −20.3 | −7.2 |
| CVP8-1 4.4 | Calcite | Cavity-filling | −16.7 | −3.9 |
| CVP8-1 4.5 | Calcite | Cavity-filling | −21.0 | −1.9 |
| CVP8-1 4.6 | Calcite | Cavity-filling | −21.0 | +4.4 |
| CVP8-1 4.7 | Calcite | Cavity-filling | −21.2 | −0.5 |
| CVP8-1 4.8 | Calcite | Cavity-filling | −19.8 | −5.9 |
| CVP8-1 4.9 | Calcite | Cavity-filling | −20.3 | −5.3 |
| CVP8-1 4.10 | Calcite | Cavity-filling | −15.5 | +3.9 |
| CVP8-2 10.2 | Calcite | Cavity-filling | −21.9 | +1.8 |
| CVP8c | Calcite | Cavity-filling | −19.8 | −4.1 |
| CVP6 | Calcite | Cavity-filling | −18.0 | −5.7 |
| CVP12a | Calcite/Dolomite | Cavity-filling | −22.4 | −1.9 |
| CVP13 | Calcite/Dolomite | Carbonate vein | −25.0 | +2.7 |
| CVP8-1 4.1 | Dolomite | Intergranular | −19.6 | −6.1 |
| CVP8a | Dolomite | Intergranular | −20.7 | +1.5 |
| CVP8b | Dolomite | Intergranular | −22.5 | +1.5 |
| CVP11a | Dolomite | Intergranular | −24.1 | −3.7 |
| CVP11b | Dolomite | Intergranular | −26.7 | −3.0 |
| CVP12b | Dolomite | Intergranular | −23.2 | −5.8 |
| *Lucina carbonates* | | | | |
| PA2 | Calcite | Intergranular | −21.9 | +6.1 |
| PA1a | Calcite | Intergranular | −20.1 | +6.5 |
| CVP7a | Calcite | Intergranular | −22.7 | +6.7 |
| PA1b | Calcite | Carbonate vein | −14.3 | −4.0 |
| CVP7b | Calcite/Aragonite | Carbonate vein | −20.7 | +0.8 |
| *Tubeworm carbonates* | | | | |
| TU1 | Calcite | Tube cluster | −24.3 | −5.6 |
| TU2 | Calcite | Tube cluster | −24.1 | +4.8 |
| RDZ1 | Calcite | Intergranular | −25.9 | +8.1 |
| RDZ3 | Calcite/Aragonite | Carbonate vein | −19.8 | +1.6 |
| ZF113A | Aragonite | Carbonate vein | −19.8 | +6.0 |

Natalicchio et al., Tab.1